A Monte Carlo simulation study of the impact of increasing the axial field of view on PET scanner sensitivity with various scintillating crystals

Abdallah El ouaridi[1]*, *Zakaria* Ait Elcadi[2], *Mounir* Mkimel[1], *Mustapha* Bougteb[1], *and Redouane* El baydaoui[1]

[1]Hassan First University of Settat, High Institute of Health Sciences, Laboratory of Health Sciences and Technologies, Settat, Morocco
[2]Electrical and Computer Engineering, Texas A&M University at Qatar, Doha, 23874, Qatar

Abstract. This study addresses sensitivity performance, a pivotal parameter of Positron Emission Tomography (PET) imaging, which measures the system's ability to detect and precisely measure radiotracer signals. It primarily depends on the scintillation material and the system's axial field of view (AFOV). Enhancing this performance can significantly increase overall system performance and clinical practice. This research evaluates the sensitivity of a simulated PET model based on different scintillation materials and extended AFOV values, following the NEMA NU 2-2018 protocol. A standard PET system model with an AFOV of 15.9 cm was developed using the GATE Monte Carlo simulation toolkit (v9.2), along with detailed modelling of the NEMA NU 2-2018 sensitivity phantom. Simulations examined six scintillation materials (BGO, GSO, LSO, LYSO, LuAP, and NaI) across AFOV sizes from 15.9 cm to 79.5 cm. Results showed a substantial increase in sensitivity with AFOV extension, following a quadratic relationship. BGO, LuAP, and LSO crystals demonstrated notable performance enhancements, while LYSO showed acceptable results. This study underscores the potential of AFOV extension and high-performance scintillation crystals to enhance sensitivity in PET scanners, thereby improving imaging quality and potentially advancing clinical practice.

1 Introduction

Positron Emission Tomography (PET) is an indispensable molecular and functional imaging technique in nuclear medicine. It is employed to ascertain various molecular and metabolic processes transpiring within the organism. It then facilitates the visualization and imaging of physiological or pathophysiological events within the human body [1]. Widely recognized as

* Corresponding author: a.elouaridi@uhp.ac.ma

the most sensitive functional imaging modality, its application spans various domains in clinical practice, including oncology, cardiology, neurology, psychiatry, and, more recently, infectiology, utilizing various positron radiotracers [2–4].

One of the PET system's most remarkable features is its sensitivity, which denotes a scanner's ability to accurately detect, visualize, and quantify even the smallest doses of radiotracers introduced into the human body. Enhancing this performance holds the promise of improving the signal-to-noise ratio (SNR) and image quality [5]. Moreover, this enhancement could lead to an optimal reduction in dose and scan time [6], which are significant challenges for this imaging modality. Two crucial aspects of PET camera instrumentation and design influence this performance: the detector material's efficiency and the scanner's shape. The efficiency of the material is primarily determined by the characteristics of the scintillation crystal, while the scanner's shape is influenced by the detector surface, which is exposed and receptive to photons (i.e., the axial field of view: AFOV) [7]. Therefore, the strategic selection of AFOV and type of scintillation crystal is a potential avenue for increasing and improving this performance.

In clinical practice, full-ring scintillation PET scanners typically cover a small solid angle, with a limited AFOV ranging from 15 to 26 cm (typically involving 3 or 5 detection rings) [8], allowing a total axial length sufficient to acquire localized PET scans, such as those of the brain or heart, in a single bed position. This length does not allow detection of the majority of gamma pairs emitted by isotopes; only 1% of all coincidence photons are detected [9]; a large part of the object is outside the axial field of view (only one-eighth of the body is actually in the scanner's field of view) [10], which has a negative influence on sensitivity performance and hampers many clinical applications requiring dynamic whole-body and parametric imaging. On the other side, various inorganic scintillator materials have been studied for PET detector design, and all of these scintillator crystals fail to respond to all the requirements of TPE detection systems [7]. For this reason, the extension of AFOV in PET scanners with an optimal crystal scintillator has received increasing attention, representing a focal point for improving the sensitivity of PET scanner performance and, subsequently, the rest of the system's performance.

In this study, we aim to investigate and quantify the influence of increasing the PET system's AFOV on sensitivity performance using Monte Carlo GATE simulations based on the NEMA NU 2-2018 protocol, emphasizing the characteristics of the various types of crystal scintillators commonly utilized in PET. To carry out this work, we simulated five distinct models of AFOV scanners with 3, 6, 9, 12 and 15 block detection rings, which we will call 3R (original), 6R, 9R, 12R and 15R. At the same time, we varied the scintillation material for this model for each AFOV value: six different candidate scintillation materials, including BGO, GSO, LSO, LYSO, LuAP and NaI. Consequently, sensitivity performance was assessed following NEMA NU 2-2018 specifications.

2 Methods

2.1 GATE simulation platform

The simulation study was conducted using the Geant4 Application for Tomographic Emission (GATE), a Monte Carlo simulation platform built upon the GEANT4 libraries (a generic Monte Carlo code) and equipped with a scripting mechanism [11]. This platform, tailored for emission tomography, allows for a detailed representation of the components essential for accurately modelling a PET system, including simulation of the system's geometry, behaviour of the radioactive source, interaction physics, scanner detectors, and

signal processing chain. Our study uses a personal computer (with an Intel Core i7-6920HQ, 2.90 GHZ) to build the scanner geometry using a GATE version of 9.2.

2.2 PET scanner simulation

The architecture of the simulated scanner was defined by a set of hierarchical elements at several depth levels. The module is the largest geometry inside the cylindrical PET, and 48 modules were arranged to form the scanner ring. Each module consists of three blocks in the axial direction. In each detector block is an array of 13 (transaxial) × 13 (axial) lutetium orthosilicate (LSO) crystals with 4 × 4 × 20 mm3. Overall, the size of each module is 53.2 mm (transaxial) × 159.8 mm (axial), covering an axial field of view (AFOV) of ~16 cm. The final configuration results in a 3-crystal ring PET scanner with a diameter of 86.4 mm. Figure 1 shows the visual representation of the simulated model in GATE. The scanner was configured with a coincidence window of 4.5 ns and an energy resolution of 11.7% (425-650 Kev window). The dead time model was set at 300 ns. Scintillation photons were digitized in GATE using a digitizer module, which is composed of several signal-processing operations, starting with adding the hits (individual photons interactions) into pulses, followed by their conversion into singles and organization into final coincidences. We simulated five distinct models of AFOV scanners with 3, 6, 9, 12, and 15 block detection rings, which we will call 3R (original), 6R, 9R, 12R, and 15R. Table 1 shows the same simulated model's axial field of view values. We also varied the scintillator material for this model: six different candidate scintillation materials, including BGO, GSO, LSO, LYSO, LuAP and NaI, and its performance in terms of sensitivity was evaluated according to NEMA NU 2-2018 specifications and with an axial field-of-view extension.

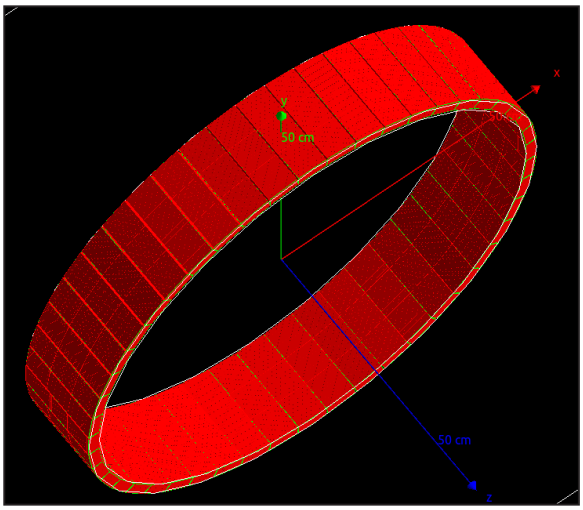

Fig. 1. Geometry of the PET system showing the configuration of three detection rings.

Table 1. The five axial field-of-view values evaluated for each crystal scintillator in the simulated scanner model.

AFOV(cm)	Scintillation materials
3 Ring =15.9	NaI
6 Ring =31.8	BGO
9 Ring =47.7	GSO
12 Ring =63.6	LSO
15 Ring =79.5	LYSO
	LuAP

2.3 Sensitivity measurements

In accordance with NEMA NU 2-2018 standards [12], we assessed the sensitivity performance of the PET scanner. Initially, we simulated a 70 cm-long polyethene phantom with inner and outer diameters of 1 mm and 3 mm, respectively, filled with a 3.4 MBq aqueous solution of 18F-FDG mixed with water. A variable number of five concentric aluminium sleeves, each with distinct inner and outer diameters (ID, OD), enveloped this phantom: 3.9-6.4 mm, 7.0-9.5 mm, 10.2-12.7 mm, 13.4-15.9 mm, and 16.6-19.1 mm (refer to Figure 2). The first acquisition commenced with the most miniature aluminium sleeves (3.9, 6.4) around the linear source, followed by the sequential addition of more extensive sleeves, and this acquisition process was repeated for each added sleeve until we obtained five acquisitions in total. These simulations, initially performed at the centre of the field of view, were then repeated at a radial distance of 10 cm. Data were acquired for each sleeve over 60 seconds. The sensitivity was calculated as:

$$sensitivity\ (Cps.KBq-1) = \frac{true\ counts\ detected}{activity \times aquisition\ time} \qquad (1)$$

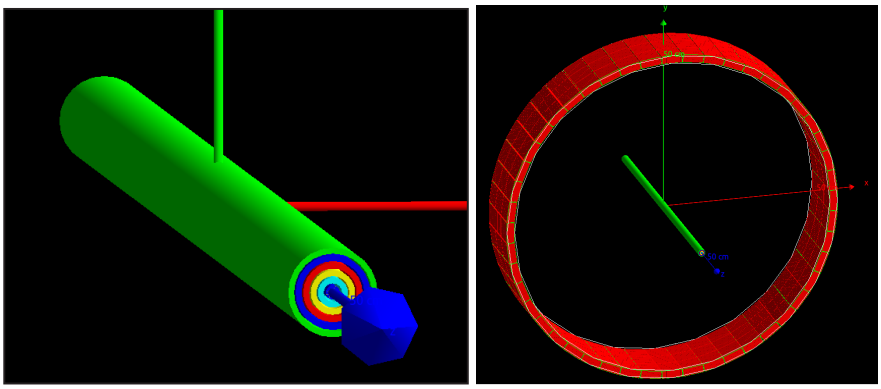

Fig. 2. View of the NEMA sensitivity phantom with GATE showing the line source inside the five concentric aluminium sleeves.

2.4 Data processing

In this work, data generated by GATE was stored in ROOT format, containing coincidence events (true, scattered, and random) and detailed information on deposited energy, annihilation positions, and detection coordinates within the modelled system. Due to ROOT's compatibility with C++, we developed a program in C++ (see Figure 3) to evaluate the system's sensitivity according to equation 1, using coincidence data from a ROOT coincidence file.

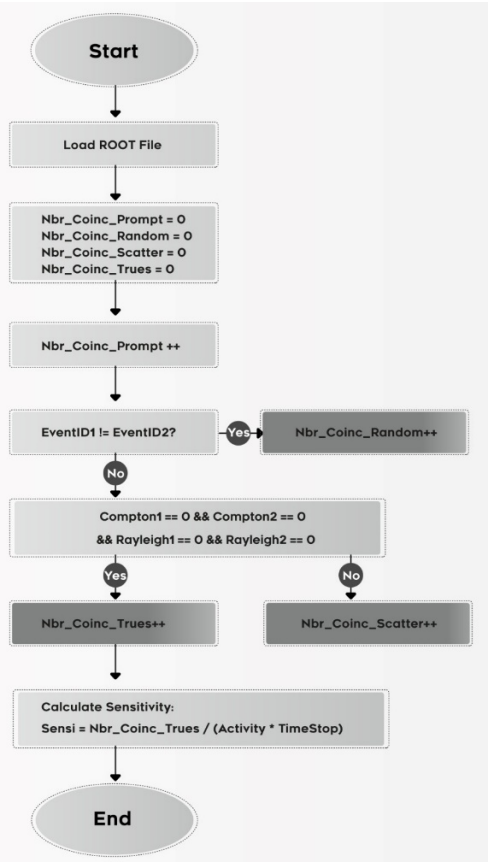

Fig. 3. Flow chart for the C++ program that counts random, scatter, and true coincidences to calculate the system's sensitivity.

3 Results

3.1 Source line image reconstruction

The source line image was reconstructed using CASToR, a flexible, open-source software platform for tomographic image reconstruction, and visualized using AMIDE, a software package specializing in visualizing medical images (as shown in the image below, Figure 4).

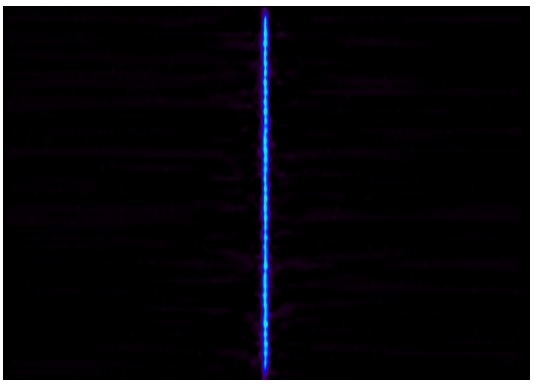

Fig. 4. The reconstructed image of the sensitivity phantom source line with its profile using AMIDE

3.2 Impact of scintillator crystal

Following processing ROOT data in MATLAB, we generated the graph below. This graph illustrates the sensitivity values of different scintillator crystals frequently employed in PET, all with a fixed AFOV of 15.9 cm.

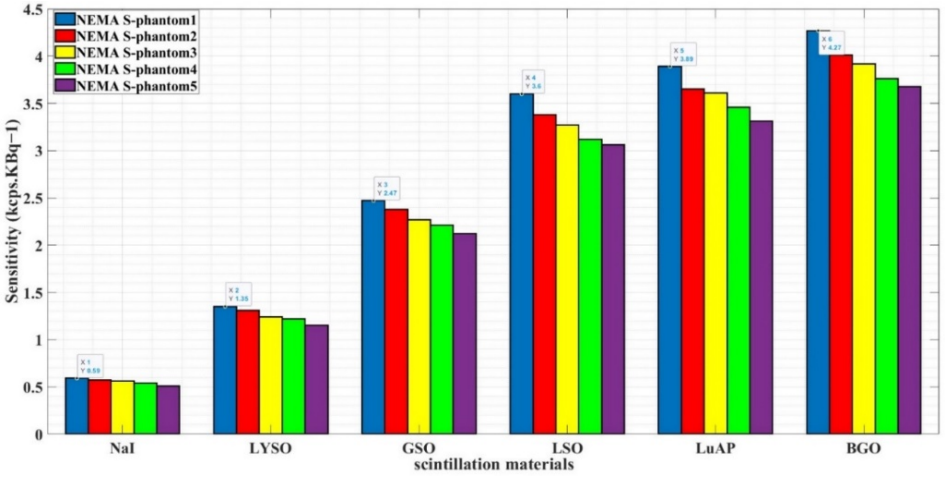

Fig. 5. Sensitivity values for various crystals and NEMA phantoms (aluminium sleeves) used (NEMA S- phantom: NEMA sensitivity phantom).

3.3 Impact of increasing axial field of view (AFOV) in PET

The AFOV was expanded for each scintillator crystal to investigate and quantify its impact on the sensitivity performance of the PET scanner. The simulation outcomes are depicted in Figure 6. A focus on LSO crystal behavior (more clinically useful) with increasing AFOV (see Figure 7).

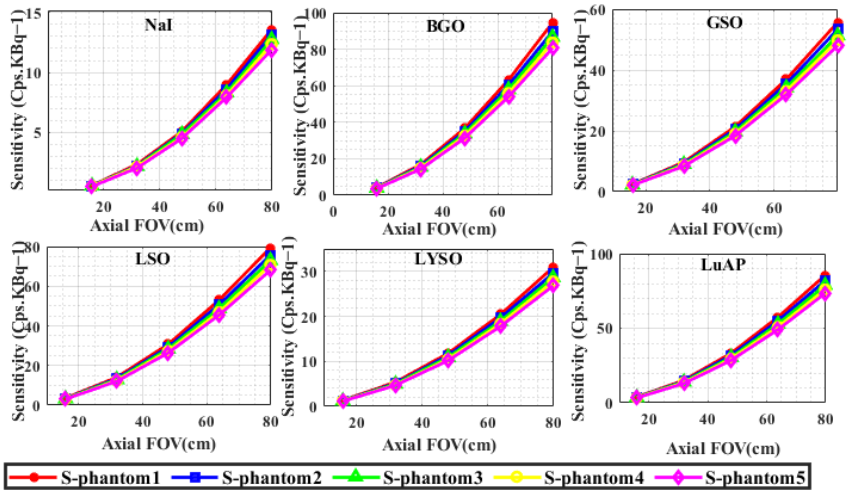

Fig. 6. Evolution of sensitivity (S) performance as a function of AFOV (S- phantom: sensitivity phantom).

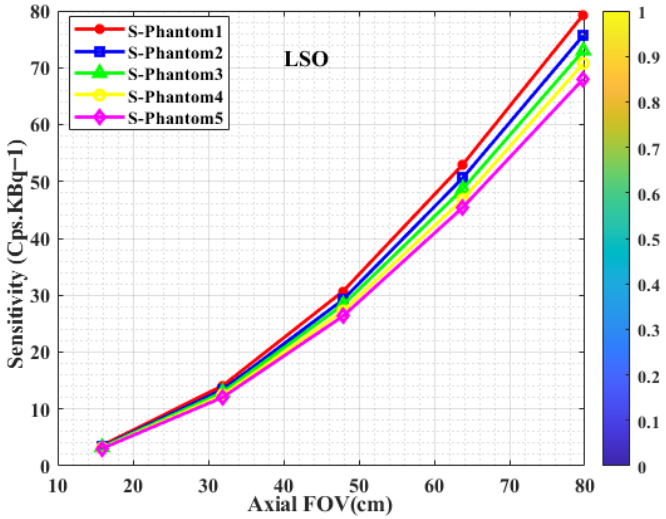

Fig. 7. Evolution of sensitivity(S) performance with LSO as a function of (AFOV)

4 Discussion

This study evaluates sensitivity performance as a function of the axial field of view while highlighting the different scintillation crystals commonly used in PET detection instrumentation. Our results indicate that a maximum value of scanner sensitivity was obtained with crystals of the BGO, LuAP and LSO types (as shown in Figure 5). In contrast, other crystals, such as GSO and LYSO, exhibited an average performance, while NaI recorded the lowest value (0.5 cps/KBq) under the same axial field of view (15.9 cm). This variance can be justified by the differences in density and atomic number of these crystals; higher atomic numbers and densities translate into higher attenuation of 511 Kev photons and better detection of true coincidences (sensitivity). This photon attenuation criterion is considered a critical parameter in the optimal choice of scintillator crystal for PET scanners

to achieve the best possible sensitivity; that is why BGO and LSO crystals have emerged as the detectors of choice for PET scanners due to their greater stopping power for the **γ** photon of 511 Kev. Although LuAP offers good sensitivity performance, as illustrated in Figure 5, it has yet to be adopted for PET due to its low luminosity and manufacturing cost [13]. These constraints limit the use of this type of crystal in clinical PET applications [13]. For LYSO, which belongs to the family of cerium-doped lutetium-based crystals, a variant of LSO in which lutetium is partially replaced by yttrium (a mixed compound); a remarkable variation in sensitivity was observed. This is explained by the fact that replacing a small amount of lutetium with yttrium affects density [7]. NaI crystal, which was used in the first generations of PET scanners, offers lower stopping power and, therefore, much lower sensitivity, making it no longer used in current clinical PET [14].

To meet all the requirements of PET detection systems, no single scintillator crystal among all those mentioned can be selected as the ideal crystal. Therefore, LSO and BGO crystals are considered the best choices because they provide sufficient stopping power. However, it is important to note that this study does not address all essential characteristics and properties of scintillator crystals. Key factors such as light yield, decay time, energy resolution, and time resolution still needed to be fully explored. Additional properties that warrant consideration include crystal transparency at the emission spectrum wavelength, refractive index, linearity, hygroscopic behaviour, as well as practical aspects like manufacturing constraints and cost.

The simulation results also illustrate the impact of AFOV on sensitivity performance for these different scintillator crystals and the phantoms used (consisting of five concentric aluminium sleeves). As anticipated, we observed a significant enhancement in sensitivity with an increased AFOV. This sensitivity variation follows a quadratic function (as shown in Figure 7); a twofold increment in AFOV results in roughly fourfold initial sensitivity improvement, and tripling, quadrupling, or quintupling the AFOV results in 11, 15, and 22 times the initial sensitivity, respectively. These significant increases in sensitivity can be explained by incorporating additional detection rings, which increase scanner coverage in the axial direction and, consequently, significant detection of true coincidences in the PET scanner's field of view. Several previous works and studies confirm this [8, 15-21]. This simulation study effectively demonstrates this AFOV-sensitivity relationship while highlighting the different scintillator crystals studied for PET detector design.

The present work evaluated the sensitivity of a PET model simulated with GATE and highlighted the interaction of two critical instrumental factors (choosing an efficient scintillator crystal and increasing the axial field of view (AFOV)) to improve scanner sensitivity significantly. However, assessing the practical interest of this newly proposed system requires additional simulations that consider not only sensitivity but also spatial resolution, image quality, and other critical aspects such as random, scattered, multiple coincidences, and dead time effects. A complete evaluation using a valid PET system model in clinical practice will be required.

5 Conclusion

This article presents the preliminary results of evaluating the impact of increasing the axial field of view (AFOV) on the sensitivity performance of a PET scanner with different scintillation crystals proposed in the literature for this medical imaging modality. Following the NEMA NU 2-2018, the scanner sensitivity was simulated and evaluated as a function of these proposed crystals and the axial field of view. Among the materials tested, BGO, LuAP, and LSO are the best-performing materials, offering the highest sensitivity under identical axial field-of-view conditions. The extension of the AFOV has considerably boosted this performance. This study highlights the significant impact of increasing axial fields of view

for PET scanners using denser crystals. This design represents a transformative step in PET imaging that could change the current paradigm of human PET imaging.

References

1. Jiang, Chalich, and Deen, 'Sensors for Positron Emission Tomography Applications', Sensors, vol. 19, no. 22, p. 5019, Nov. 2019, doi: 10.3390/s19225019.
2. D. L. Bailey, Ed., Positron emission tomography: basic sciences. New York: Springer, 2005.
3. C. K. Hoh, 'Clinical use of FDG PET', Nucl. Med. Biol., vol. 34, no. 7, pp. 737–742, Oct. 2007, doi: 10.1016/j.nucmedbio.2007.07.001.
4. J. P. Pijl, T. C. Kwee, R. H. J. A. Slart, and A. W. J. M. Glaudemans, 'PET/CT Imaging for Personalized Management of Infectious Diseases', J. Pers. Med., vol. 11, no. 2, p. 133, Feb. 2021, doi: 10.3390/jpm11020133.
5. A. Dimitrakopoulou-Strauss, L. Pan, and C. Sachpekidis, 'Long axial field of view (LAFOV) PET-CT: implementation in static and dynamic oncological studies', Eur. J. Nucl. Med. Mol. Imaging, Apr. 2023, doi: 10.1007/s00259-023-06222-3.
6. L. R. MacDonald, R. L. Harrison, A. M. Alessio, W. C. J. Hunter, T. K. Lewellen, and P. E. Kinahan, 'Effective count rates for PET scanners with reduced and extended axial field of view', Phys Med Biol, no. 56, pp. 3629–3643, 2011, doi: doi:10.1088/0031-9155/56/12/011.
7. A. El Ouaridi, Z. Ait Elcadi, M. Mkimel, M. Bougteb, and R. El Baydaoui, 'The detection instrumentation and geometric design of clinical PET scanner: towards better performance and broader clinical applications', Biomed. Phys. Eng. Express, vol. 10, no. 3, p. 032002, May 2024, doi: 10.1088/2057-1976/ad2d61.
8. J. K. Poon et al., 'Optimal whole-body PET scanner configurations for different volumes of LSO scintillator: a simulation study', Phys. Med. Biol., vol. 57, no. 13, pp. 4077–4094, Jul. 2012, doi: 10.1088/0031-9155/57/13/4077.
9. S. Vandenberghe, P. Moskal, and J. S. Karp, 'State of the art in total body PET', EJNMMI Phys., vol. 7, no. 1, p. 35, Dec. 2020, doi: 10.1186/s40658-020-00290-2.
10. E. Berg and S. R. Cherry, 'Innovations in Instrumentation for Positron Emission Tomography', Semin. Nucl. Med., vol. 48, no. 4, pp. 311–331, Jul. 2018, doi: 10.1053/j.semnuclmed.2018.02.006.
11. G. Santin et al., 'GATE, a Geant4-based simulation platform for PET integrating movement and time management', in 2002 IEEE Nuclear Science Symposium Conference Record, Norfolk, VA, USA: IEEE, 2003, pp. 1325–1329. doi: 10.1109/NSSMIC.2002.1239563.
12. National Electrical Manufacturers Assoc, 'Performance measurements of positron emission tomographs. NEMA Standards Publication NU 2-2018.', Rosslyn USA, 2018.
13. A. Ghabrial, D. Franklin, and H. Zaidi, 'A Monte Carlo simulation study of the impact of novel scintillation crystals on performance characteristics of PET scanners', Phys. Med., vol. 50, pp. 37–45, Jun. 2018, doi: 10.1016/j.ejmp.2018.05.010.
14. G. B. Saha, Basics of PET Imaging: Physics, Chemistry, and Regulations. Cham: Springer International Publishing, 2016. doi: 10.1007/978-3-319-16423-6.

15. S. Surti, M. E. Werner, and J. S. Karp, 'Study of PET scanner designs using clinical metrics to optimize the scanner axial FOV and crystal thickness', Phys. Med. Biol., vol. 58, no. 12, pp. 3995–4012, Jun. 2013, doi: 10.1088/0031-9155/58/12/3995.
16. J. K. Poon, L. R. MacDonald, S. R. Cherry, and R. D. Badawi, 'A Simulation Study of aLong Axial Field of View Whole-Body PET Scanner using Cylindrical and Anthropomorphic Phantoms', IEEE, vol. 978, no. 1, pp. 4999–5006, 2008.
17. R. D. Badawil, S. G. Kohlmyer', R. L. Harrison', S. D. Vannoy', and T. K. Lewellen', 'The Effect of Camera Geometry on Singles Flux, Scatter Fraction and Trues and Randoms Sensitivity for Cylindrical 3D PET - a Simulation Study.', IEEE TRANSACIIONS Nucl. Sci., vol. 47, no. 3, pp. 1228–1232, Jun. 2000.
18. S. Surti, E. Lee, M. E. Werner, and J. S. Karp, 'Imaging study of a clinical PET scanner design using an optimal crystal thickness and scanner axial FOV', in 2011 IEEE Nuclear Science Symposium Conference Record, Valencia, Spain: IEEE, Oct. 2011, pp. 3390–3394. doi: 10.1109/NSSMIC.2011.6152615.
19. L. Eriksson et al., 'Potentials for large axial field of view positron camera systems', in 2008 IEEE Nuclear Science Symposium Conference Record, Dresden, Germany: IEEE, Oct. 2008, pp. 1632–1636. doi: 10.1109/NSSMIC.2008.4775110.
20. S. Karp, G. Muehllehner, and P. Countryman, 'Effect of Increased Axial Field of View on the Performance of a Volume PET Scanner', IEEE Trans. Med. IMAGING, vol. 12, no. 2, 1993.
21. L. Eriksson et al., 'An investigation of sensitivity limits in PET scanners', Nucl. Instrum. Methods Phys. Res. Sect. Accel. Spectrometers Detect. Assoc. Equip., vol. 580, no. 2, pp. 836–842, Oct. 2007, doi: 10.1016/j.nima.2007.06.112.